Available online at www.sciencedirect.com

ScienceDirect

Advances in Space Research 59 (2017) 1526–1538

ADVANCES IN SPACE RESEARCH (a COSPAR publication)

www.elsevier.com/locate/asr

Characteristics of equatorial electrojet derived from Swarm satellites

Neethal Thomas *, Geeta Vichare, A.K. Sinha

Indian Institute of Geomagnetism, Plot 5, Sector 18, New Panvel (W), Navi Mumbai 410218, India

Received 21 January 2016; received in revised form 15 December 2016; accepted 16 December 2016
Available online 26 December 2016

Abstract

The vector magnetic field measurements from three satellite constellation, Swarm mission (Alpha 'Swarm-A', Bravo 'Swarm-B', and Charlie 'Swarm-C') during the quiet days (daily $\sum \mathrm{Kp} \leqslant 10$) of the years 2014–2015 are used to study the characteristic features of equatorial electrojet (EEJ). A program is developed to identify the EEJ signature in the X (northward) component of the magnetic field recorded by the satellite. An empirical model is fitted into the observed EEJ signatures separately for both the hemispheres, to obtain the parameters of electrojet current such as peak current density, total eastward current, the width of EEJ, position of the electrojet axis, etc. The magnetic field signatures of EEJ at different altitudes are then estimated. Swarm B and C are orbiting at different heights (separation ~50 km) and during the month of April 2014, both the satellites were moving almost simultaneously over nearby longitudes. Therefore, we used those satellite passes to validate the methodology used in the present study. The magnetic field estimates at the location of Swarm-C obtained using the observations of Swarm B are compared with the actual observations of Swarm-C. A good correlation between the actual and the computed values (correlation coefficient = 0.98) authenticates the method of analysis. The altitudinal variation of the amplitude and the width of the EEJ signatures are also depicted. The ratio of the total eastward flowing forward to westward return currents is found to vary between 0.1 and 1.0. The forward and return current values in the northern hemisphere are found to be ~0.5 to 2 times of those in the southern hemisphere, thereby indicating the hemispheric asymmetry. The latitudinal extents of the forward and return currents are found to have longitudinal dependence similar to that of the amplitude and the width of EEJ showing four peak structures. Local time dependence of EEJ parameters has also been investigated. In general, the results are found to be consistent with previous studies. In order to examine the existence of the EEJ associated meridional currents, we have estimated the vertical current density using combination of two satellites separated in longitude.

Keywords: Equatorial electrojet; Swarm magnetic field; EEJ current parameters; Characteristics of equatorial electrojet currents

1. Introduction

The E-region ionosphere is a dynamo layer, where the atmospheric neutral winds cause charge particles to move across the magnetic field resulting in electric fields and currents. The primary eastward electric fields together with the horizontal geomagnetic field at the dip equator cause Hall and Pederson currents to flow in a narrow altitudinal region bounded by the neutral atmosphere below and collisionless plasma above, causing strong vertical electric fields. This vertical electric field produces large eastward Hall current, thereby greatly enhancing the net eastward current. This intense eastward jet current flowing during daytime in the E-region ionosphere (altitude ~106 km) at the dip equator is called equatorial electrojet (EEJ) (Chapman, 1951; Onwumechili, 1997).

The study of EEJ has been extensively carried out for several decades using various observational platforms and models (Forbes, 1981 and references therein,

* Corresponding author.
E-mail addresses: neethalmariyathomas@gmail.com (N. Thomas), vicharegeeta@gmail.com (G. Vichare), sinha.ashwini@gmail.com (A.K. Sinha).

http://dx.doi.org/10.1016/j.asr.2016.12.019
0273-1177/

Onwumechili, 1997). Different observational platforms used for EEJ studies include ground based observations, sounding rockets and satellites- each one having its own advantages and limitations. The ground based observations (Fambitakoye and Mayaud, 1976; Raghavarao and Anandarao, 1987; Rastogi et al., 2007) record the temporal variations of the magnetic field over a particular location, but they lack in spatial coverage as many of the areas around the globe is covered by forest and oceans. Satellites, on the other hand, record the magnetic field variations revolving around the earth in different orbits at different altitudes. Among different satellites, the polar low earth orbiting (LEO) satellites (Cain and Sweeney, 1973; Jadhav et al., 2002; Lühr et al., 2004, 2008; Alken and Maus, 2007) have the advantage of true spatial coverage, as it covers the entire globe in a day. However, on a given day, because of the rapid motion, these satellites lack in recording the diurnal geomagnetic field variations caused by quiet-time ionospheric currents. Both ground and satellite measurements give the height integrated effect of ionospheric/magnetospheric currents, whereas rockets (Sastry, 1970; Sampath and Sastry, 1979; Onwumchili, 1992; Chandra et al., 2000) are the only means to get height profile of the ionospheric currents. However, the rocket cannot record the spatial and temporal variations. Apart from observations, different theoretical and numerical models were also developed to address physical features of EEJ (Sugiura and Cain 1966; Untiedt 1967; Sugiura and Poros 1969; Richmond 1973; Stenning 1985).

Polar LEO satellite observations are distinctly advantageous in EEJ studies as they provide the global observation of the current system, by spanning the currents latitudinally and longitudinally on a given day. POGO was the first polar LEO mission to show the signature of the EEJ currents as a negative depression in the magnetic field over equatorial latitudes (Cain and Sweeny, 1973; Onwumechili and Agu, 1980; McCreadie, 2004). POGO was followed by Magsat, a sun-synchronized satellite in the dawn-dusk orbit. It provided the first evidence of the existence of meridional currents associated with EEJ in the equatorial ionosphere (Maeda et al., 1982). Jadhav et al. (2002) and Ivers et al. (2003) studied the characteristic of EEJ current system in detail by using the total magnetic field measurement from Ørsted satellite. Jadhav et al. (2002) estimated the EEJ parameters like peak current density, total current, and the width of the current system using Ørsted data. They found that the EEJ strength estimated at ground using satellite data correlate well with EEJ observations from Indian and American ground observatories. Later, Lühr et al. (2004) deduced the characteristics of the EEJ currents using scalar magnetic field measurements from CHAMP, thereby reaffirming the results from Ørsted. To derive a global picture of EEJ, Alken and Maus (2007) developed the climatological model of EEJ, using the scalar magnetic field measurements from Ørsted, CHAMP, and SAC-C satellites. Using this empirical model, they estimated the local time (LT), longitudinal and seasonal dependence of EEJ current. Lühr et al. (2008) made use of this model in estimating the influence of non-migrating DE3 tidal mode on the intensity of EEJ. The reverse electrojet phenomenon, known as the Counter Electrojet (CEJ) is also reported in the scalar magnetic field measurements at Ørsted by Vichare and Rajaram (2011). They delineated the characteristics of the global distribution of CEJ by investigating its longitudinal, LT and seasonal dependence. The magnetic field data from all these earlier LEO missions have been analysed by different methods by different researchers for e.g. Jadhav et al. (2002) fitted Onwumchilli's empirical model of EEJ currents into the magnetic field observations, while Lühr et al. (2004) fitted a series of line currents. However, the broad features of the EEJ obtained from independent methods are consistent.

In the present paper, we have derived global features of EEJ by fitting empirical model in the X-component of the magnetic field obtained from the recently deployed polar LEO mission satellites Swarm. Further, in order to examine the vertical extent of the EEJ associated currents, we have estimated the F-region currents using Ampere's equation. It is found that vertical currents may be associated with the F-region dynamo. The paper is organized as follows. Section 2 presents the data and identification of EEJ signatures. Section 3 describes the empirical model of EEJ and the method of analysis used in the present study for deriving the EEJ current parameters. The section also presents the results such as altitudinal variation of EEJ signatures, the characteristics of forward and return currents of EEJ, the longitudinal and LT variation of the EEJ. Section 4 presents the F-region currents. Finally, the results are discussed and summarized in Section 5.

2. Data set and identification of EEJ signature

European space agency (ESA)'s multi-satellite mission Swarm, consist of three identical satellites namely Alpha (Swarm-A), Bravo (Swarm-B) and Charlie (Swarm-C). The satellites were launched together in November 2013 into a near-polar orbit with inclination >87°. Later in January 2014, the spacecrafts were moved into different orbits and attained the final constellation in April 2014. Swarm-A and Swarm-C orbits side by side at an altitude of ~460 km, whereas Swarm-B moves at a higher altitude of ~520 km. With a higher inclination orbit, Swarm-B drifts longitudinally from Swarm-A & C by 20° in every year. All the three satellites complete one orbit in ~90 min duration and hence constitute nearly 15 day and night passes each in 24 h. Drifting slowly in LT by ~1 h in every 11 days, satellites witnesses all LT sectors in nearly 4 months duration.

The present study utilizes the vector magnetic field measurements in NEC (North East Centre) frame from fluxgate magnetometer onboard satellites Swarm-B and Swarm-C for a period of one and half year from January 2014 to June 2015. The dataset used is Level 1b magnetic product: MAGX_LR_1B with 1 Hz sampling rate. As we are interested in investigating the EEJ characteristics, only satellite passes during geomagnetic quiet periods with daily $\sum Kp \leqslant 10$ in the LT range 0900–1500 h are considered. In order to separate the magnetic field variations due to ionospheric currents, the main field model, CHAOS 5 (Finlay et al., 2015), is subtracted from magnetic field recorded by Swarm. CHAOS 5 accounts for the internal (core and crustal) field, its secular variation and acceleration. It also accounts for the magnetic field contributions from static magnetospheric currents and time varying ring currents. The residual fields so obtained contain magnetic field contributions from various ionospheric currents. In order to identify clear EEJ signatures from the residuals, the contribution of other ionospheric currents such as solar quiet (Sq) has to be removed. This is achieved by fitting a polynomial of degree 5 on the latitudinal profile of the residual fields excluding $\pm 14°$ dip latitudes. The fitted polynomial is then subtracted from the data to obtain the magnetic field variations caused by equatorial ionospheric currents. As EEJ current flows in the east-west direction in a narrow latitudinal region near dip equator, the residual magnetic field variations in X component within $\pm 20°$ dip latitudes is only considered in this study. A total of 1115 daytime satellite passes from over 70 days were obtained from the considered quiet period and are further analyzed to identify the EEJ signatures.

A typical EEJ signature monitored by polar LEO satellite marks a minimum in the magnetic field value near the dip equator followed by two maxima on either side (Cain and Sweeny, 1973; Jadhav et al., 2002; Lühr et al., 2004).

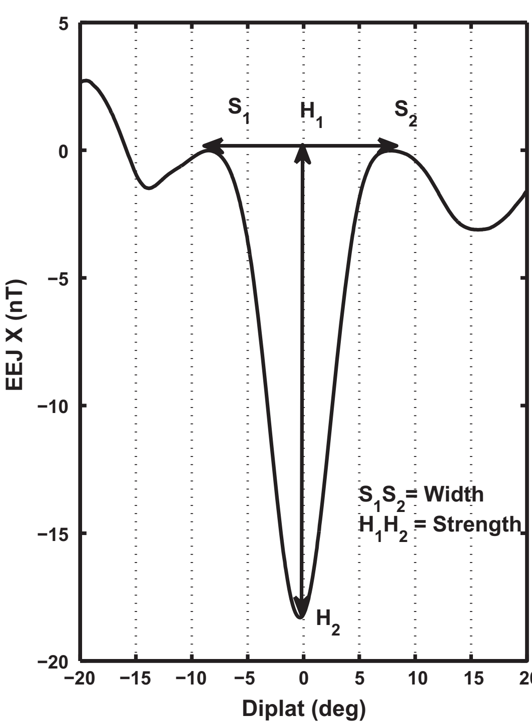

Fig. 1. Latitudinal profile of EEJ identified in Swarm-B measurements during its pass over 162°E longitude at 1141 LT.

Fig. 1 depicts a typical EEJ signature observed by the Swarm-B satellite. Although this typical signature of EEJ is presented in a few previous research papers, we are presenting it again as it would help the readers to know the parameters used in the present study. The two maxima denoted by S_1 and S_2 mark the edge of the EEJ and are hereafter called as the shoulders. These shoulders can be assumed to represent the signatures of the EEJ return currents in the magnetic field measurements. In Fig. 1, the width and the amplitude of EEJ signature are marked as S_1S_2 and H_1H_2 respectively. For each satellite pass, the latitudinal profile of EEJ is identified by a completely automated program. As the EEJ signature varies from pass to pass, the program also considers the signatures those deviate slightly from the typical signatures of EEJ. Sometimes, there is an absence of a well-defined maximum in one of the hemispheres, or sometimes there is no clear signature of the maxima, instead there is only a change in slope. Such situations are also considered by the developed program. The criteria used for selecting the EEJ signature are adopted from Jadhav et al. (2002) (Section 2 in their paper) and are described as follows. (1) The Presence of a well-defined minimum within $\pm 2°$ of the dip equator, (2) minimum followed by two well-defined maxima- one on either side. (3) If only one well-defined maximum is present, the other is considered to be at a symmetrically opposite point with respect to the location of the minimum. (4) The maxima identified only as a change in slope, are also considered as a shoulder.

Following this criteria, nearly 984 satellite passes for each satellite were identified with EEJ signatures and are investigated further.

3. Study of EEJ using empirical model

3.1. Methodology

The magnetic signatures of EEJ with a depression near dip equator and the shoulders on both the flanks observed by the satellite are considered to have resulted from the eastward current flowing near the dip equator and the westward return currents on either side flowing below the satellite altitude in the E-region (Onwumechilli, 1992). An empirical model based on the continuous distribution of current density for EEJ given by Onwumechili (1997) is fitted to the electrojet signatures identified in the X component of the magnetic field recorded by the satellite. According to the model, the current density at a point (x, z) is given by

$$j = j_0 \frac{a^2(a^2 + \alpha x^2)}{(a^2 + x^2)^2} \frac{b^2(b^2 + \beta z^2)}{(b^2 + z^2)^2} \tag{1}$$

With the center of the current system as the origin, x is the latitudinal distance positive in the northward direction, y is positive eastward and z is the vertical distance from the current layer positive downwards. Here, a and b are the scale lengths and α and β are dimensionless constants controlling the distribution of currents along x and z respectively. j_0 is the peak current density at $x = 0$ and $z = 0$. The height integrated current density or the current intensity, J is given by

$$J = J_0 \frac{a^2(a^2 + \alpha x^2)}{(a^2 + x^2)^2} \tag{2}$$

where J_0 is the peak current intensity in A/km. The northward component of the magnetic field $EEJ\text{-}X$ (in nT) caused by this east-west thin current sheet is given as

$$EEJ\text{-}X = \frac{Ka}{2(sg.z)P^4}[(v + \alpha v + 2\alpha a)(u + b)^2 + (v + \alpha v + 2a)(v + a)^2] \tag{3}$$

where
$P^2 = (u + b)^2 + (v + a)^2$,
$K = 0.2\pi J_0$ is the magnetic constant in nT,
$u = |x|$, $v = |z|$, $sg.z = sign\ of\ z = \frac{z}{v}$

Considering that the current is flowing at 106 km altitude and taking $b = 0$, the magnetic field variation resulting from this current sheet at satellite locations (x, z) within $\pm 20°$ latitudes is estimated using Eq. (3). In practice, the height of the EEJ current may vary within 106 ± 4 km, though it is assumed to be at 106 km in the present study. Here, the three unknown values α, a and K which define the shape, width and amplitude respectively of the electrojet signature are estimated by an iterative method as described by Jadhav et al. (2002). In the present study, in order to get a more realistic estimate of EEJ, the values of α and a are estimated separately for both the hemispheres, unlike Jadhav et al. (2002), who assumed it to be symmetric. With values of α, a, and K identified that provide a best fit in the actual observations, EEJ can now be estimated at any altitude. The procedure is completely automated and is performed for all satellite passes those exhibit discernible EEJ signatures.

We firstly validate the reliability of the method adopted here in identifying the EEJ parameters. This is done by estimating X variations at Swarm-C using the measurements from overhead Swarm-B satellite pass, and comparing with the actual observations from Swarm-C satellite. EEJ-X at Swarm-C is computed using the model values identified by fitting the EEJ model to the Swarm-B observations. Swarm-B and Swarm-C which are orbiting at two different altitudes came close in longitude during the month of April 2014. In this period, there were several passes for which Swarm-B and C were almost over identical longitudes (<5°) with nearly identical universal time (UT) (difference <~3 min). Here, we have restricted the data to this period during which Swarm-B and Swarm-C were passing one above the other. We obtained 52 such satellites passes for which comparison is made.

Fig. 2, shows the comparison between the amplitudes of EEJ calculated (EEJ-$X_{Calculated}$) and observed (EEJ-$X_{Observed}$) at Swarm-C. The scatter shows a linear variation with the fitted linear regression line having slope 1. The correlation coefficient (CC) between the EEJ amplitudes calculated and observed at Swarm-C satellite is found to be 0.98. The excellent match between the EEJ amplitudes obtained from the direct observations and the model validates the technique adopted here.

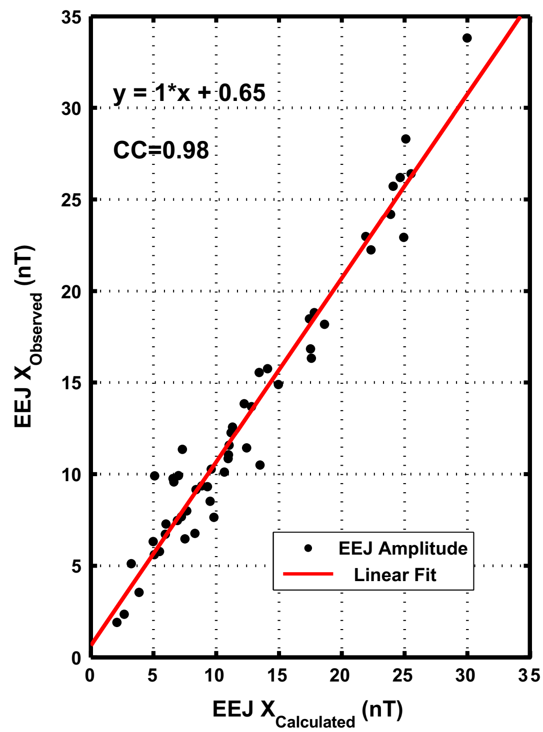

Fig. 2. Scatter plot of observed and estimated EEJ amplitude at Swarm-C.

3.2. EEJ current parameters

The EEJ parameters studied here are:

(1) the peak current density J_0, expressed by

$$J_0 = \frac{K}{(0.2 \times \pi)} \tag{4}$$

(2) the total eastward current I_+, given by

$$I_+ = I_{+(NH)} + I_{+(sH)} \tag{5}$$

where

$$I_{+(SH)} = \frac{a_{SH} J_0}{2}\left[(-\alpha_{SH})^{1/2} + (1 + \alpha_{SH}) \tan^{-1}\left(\frac{1}{-\alpha_{SH}}\right)^{1/2}\right] \tag{5a}$$

$$I_{+(NH)} = \frac{a_{NH} J_0}{2}\left[(-\alpha_{NH})^{1/2} + (1 + \alpha_{NH}) \tan^{-1}\left(\frac{1}{-\alpha_{NH}}\right)^{1/2}\right] \tag{5b}$$

(3) the full width ($W_{Current}$) of the current sheet,

$$W_{Current} = W_{Current(SH)} + W_{Current(NH)} \quad (6)$$

where

$$W_{Current(SH)} = \frac{a_{SH}}{\sqrt{-\alpha_{SH}}} \quad (6a)$$

$$W_{Current(NH)} = \frac{a_{NH}}{\sqrt{-\alpha_{NH}}} \quad (6b)$$

and (4) the location of the electrojet axis with respect to the dip equator, i.e., the dip latitude at which EEJ peaks. Here, α_{NH} and a_{NH} denotes α and a in the northern hemisphere and similarly α_{SH} and a_{SH} denotes that in the southern hemisphere.

These four current parameters are estimated for all the considered passes of Swarm-B and are compared with the amplitude and width of EEJ estimated at ground using the model values. The statistics are portrayed in Fig. 3. Fig. 3a shows the linear relationship between the peak current density (J_0) and EEJ amplitude calculated at ground (EEJ-X_{Ground}) with a good correlation of 0.94. The total eastward current (I_+) also showed a clear linear dependence with the EEJ amplitude at ground (Fig. 3b). Here, the scatter is found to be less with an increased correlation of 0.97 compared to that of J_0 thereby indicating that I_+ better decides the EEJ signatures at ground compared to J_0. Fig. 3c shows the dependence of the location of the electrojet axis (x_0) on the EEJ amplitude at ground. It is observed that the EEJ strength is smaller for the current axis located away from the dip equator i.e., weak EEJ appears to deviate from the dip equator. In Fig. 3d, the relationship between peak current intensity and the width of EEJ at current height is shown. There are a few previous reports which show the inter-dependence of these parameters. Although Lühr et al. (2004) could not find a good correlation between these two parameters; they reported that EEJs with higher current densities can have larger widths. On the other hand, Jadhav et al. (2002) concluded that smaller current densities can have larger widths. However, our results (Fig. 3d) do not show any systematic dependence of the width of EEJ on peak current intensity. Analysis of larger data set may throw some light on this relationship.

In general, the EEJ parameters estimated using Swarm measurements are consistent with those obtained using Ørsted (Jadhav et al., 2002) and CHAMP (Lühr et al., 2004) satellite data.

3.3. Altitudinal variation of EEJ signatures

Altitudinal variation of EEJ parameters such as amplitude and width are investigated using Swarm-B and Swarm-C observations along with the fitted empirical model of EEJ. The observations are shown in Fig. 4. Here, the satellite passes of Swarm-B and Swarm-C are selected

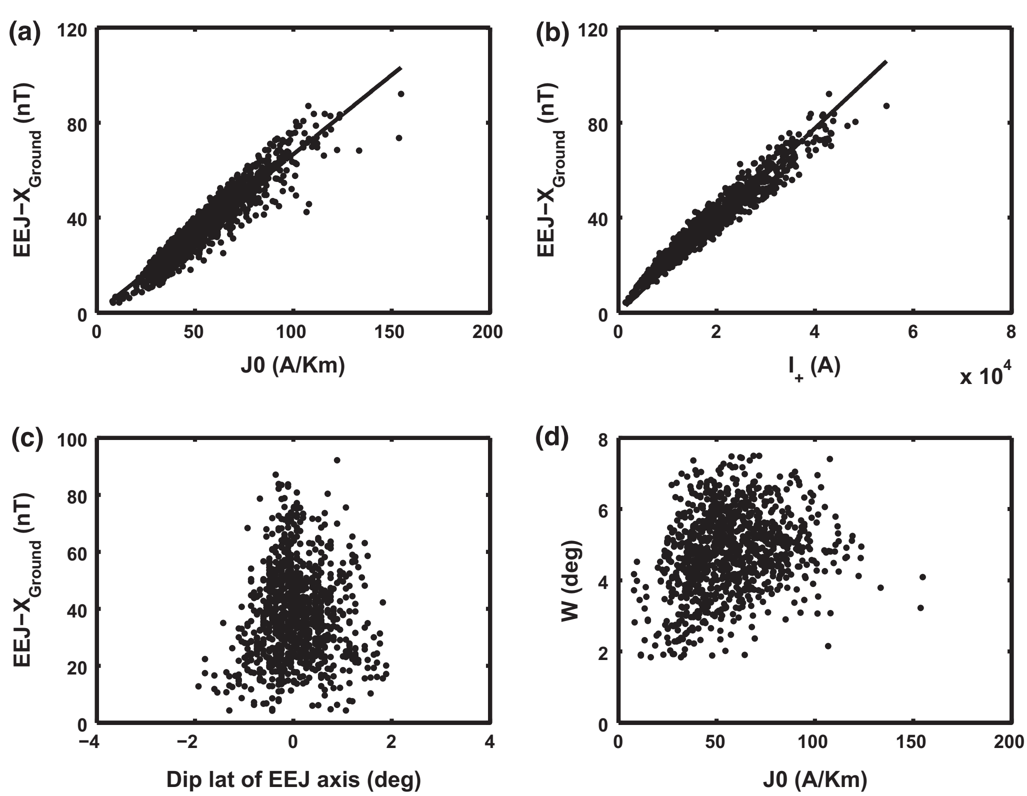

Fig. 3. Comparison of EEJ current parameters with EEJ estimated at ground. Different panels show the variation of EEJ amplitude at the ground with (a) peak current density, (b) total eastward current with and (c) EEJ current axis and (d) the variation of EEJ current width with peak current intensity.

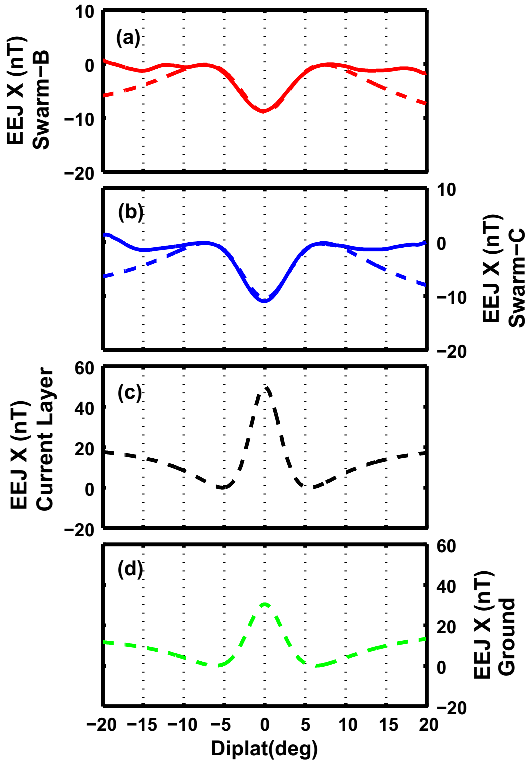

Fig. 4. EEJ signature estimated (dashed line) at (a) Swarm-B, (b) Swarm-C, (c) current height and (d) ground, using Swarm-B measurements, together with actual observations (solid line) from Swarm-B and Swarm-C.

for the period when both were orbiting one above the other at nearly identical longitudes (<3°). Arranged in the decreasing order of altitude, panels from top to bottom in Fig. 4 show EEJ-X calculated (dashed line) at locations of (a) Swarm-B, (b) Swarm-C, (c) at 105 km altitude, and (d) at ground by fitting the electrojet model to Swarm-B observations. The actual observations (solid line) from Swarm-B and Swarm-C are also shown together with the fitted profiles in Fig. 4a and b. The figure exhibits the EEJ signatures and its characteristic features such as amplitude and width, at different altitudes. With opposite sense of magnetic field directions above and below the current layer at 106 km altitude, EEJ shows inverted signatures at satellites and at locations below the current altitude. Unlike at satellites, the EEJ signature below the current layer shows a maximum near dip equator and two minima on either side, with the locations of minima marked as the shoulders of EEJ.

It is obvious to find that amplitude of EEJ depends on the distance from the current system and is clearly demonstrated in Fig. 4. EEJ shows maximum amplitude at a location just below the current layer (Fig. 4c). With increasing distance from the current sheet, it is observed that the EEJ amplitude decreases, i.e., EEJ signatures at a higher distance from the current layer are found to have smaller amplitudes. At the ground, which is 106 km below the current layer, EEJ amplitude decreases to ~0.4 times the peak value (Fig. 4d). whereas at Swarm-B (Fig. 4a) and Swarm-C (Fig. 4b), which are nearly at 4 times higher distance compared to the ground, the EEJ amplitude is found to be reduced to ~0.8 times its peak value.

The width of EEJ signature, when compared to that of amplitude, is found to have an inverse dependence on the distance from the current layer. The width of the EEJ signature is directly proportional to the distance from current layer, i.e., as the distance from the current layer increases the width of the signature also increases. EEJ signature is found to be most narrow near the current layer. At ground and satellites, the width of EEJ signature is found to increase by ~2° and ~4° respectively.

Fig. 5 shows the average variation of the (a) width and (b) amplitude of EEJ at different altitude. These two parameters were estimated using observations from Swarm-B, during April 2014 when Swarm-B and Swarm-C were moving at nearly identical longitude with a radial separation of ~50 km. The blue bars in Fig. 5a and b indicate the average values calculated using Swarm-B observations and the red bars indicate the average values of the actual observations at Swarm-C. Apart from these four discrete locations, the continuous altitude profiles of these parameters are estimated at every 5 km separations and are marked with black solid line. The average profile shows maximum amplitude and minimum width near current altitude, with amplitude (width) decreasing (increasing) with increasing distance from the current layer. The average values also show that EEJ amplitude reduces by a factor of ~0.4 at the ground and ~0.8 at the satellite with respect to the peak value. Similarly, the width of EEJ increases by ~2° at the ground and ~4° at satellite with respect to that at the current location. Thus, the amplitude and width of EEJ show an inverse relationship with altitude.

3.4. Characteristics of westward currents at off-equatorial latitudes

Fig. 6 shows the latitudinal profile of the current density derived using Eq. (2) during a noontime satellite pass. It shows the maximum eastward current density ($J_0 = \mathrm{OD}$) at dip equator and maximum westward current on both sides of the dip equator at $\sim \pm 5°$ latitudes, marked as B1 and B2, which are termed as the 'shoulders' of EEJ. Note that ideally, beyond ~ 10–15° latitude, the currents should become zero, but the profile shows an increasing trend, which could be due to improper removal of Sq contribution or bad fitting of the empirical model at those latitudes. However, the presence of westward current peaking near ±5° dip latitudes was also marked through other studies such as line current model used by Lühr et al. (2004), etc. Hence, the locations of westward currents are predicted well by present fitting. Lühr et al. (2004) considered these westward currents as an indicative of return currents of EEJ. Actually, unlike Sq currents, there is no clear evidence of closure of the EEJ current using ground magnetic field measurements, and hence it is a debatable topic (Vichare

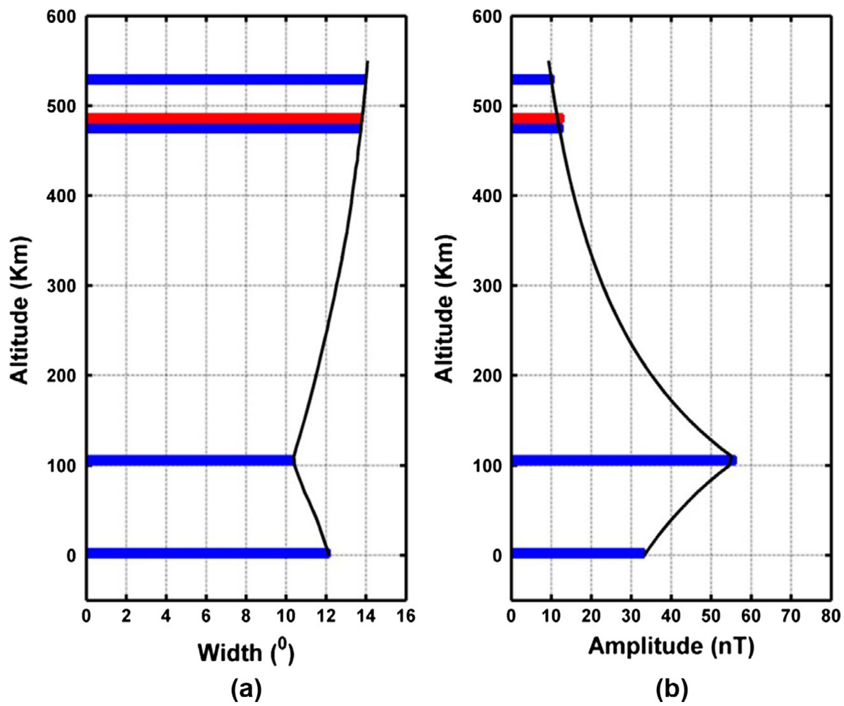

Fig. 5. Average variation of EEJ (a) width and (b) amplitude at different altitudes.

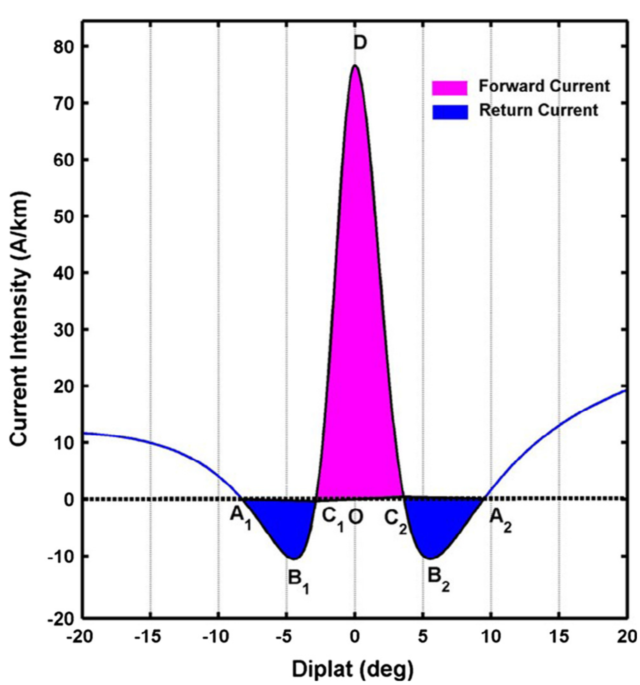

Fig. 6. Latitudinal variation of EEJ current intensity (J).

et al., 2016). Using ground, rocket, and satellite based observations, Onwumechilli (1992) reported the presence of return currents of EEJ in both hemispheres at off-equatorial latitudes, suggesting that EEJ current gets closed in a horizontal plane with westward return currents flowing at some latitudes between the dip equator and Sq foci. However, Stening (1995) proposed that these westward currents are not necessarily a part of EEJ (Stening 1995). Instead, they are caused by the vertical wind shears associated with tidal winds and gravity waves (Richmond, 1973; Reddy and Devasia, 1981; Stening, 1995]. However several studies using LEO satellites have interpreted the EEJ 'shoulders' (maxima) present on either sides of the dip equator as the signature of return (westward) currents flowing at the flanks of the EEJ (Cain and Sweeney, 1973; Jadhav et al., 2002a; Lühr et al., 2004).

We use the current density profile depicted in Fig. 6 to investigate the characteristic features of forward (eastward) and return (westward) currents of the electrojet. Lühr et al. (2004) found that the return current peaks at ±5° dip latitudes and reduces to zero level at almost 4° off the shoulder locations in both the hemispheres (their Fig. 3). In the present analysis, we adopt the similar latitudinal positions for the termination of the EEJ currents, as our profiles normally do not converge to zero as mentioned above. Therefore, we fit a dotted line passing through the points 4° beyond the shoulder locations in both the hemispheres, which is marked as zero level. In Fig. 6, the areas shaded in magenta and blue colours represent the total forward (eastward) and total return (westward) currents respectively.

The forward and return currents are estimated using all the satellite passes of Swarm-B as described above. Fig. 7a shows the variation of the return currents with peak current density (J_0). The return currents are found to vary proportional to the peak current density, implying that stronger jet currents will cause larger return current flows. Fig. 7b shows the variation of total return currents with total forward current. In general, the return current shows a linear variation with the forward current, but with a larger scatter. The slope of the fitted linear regression line

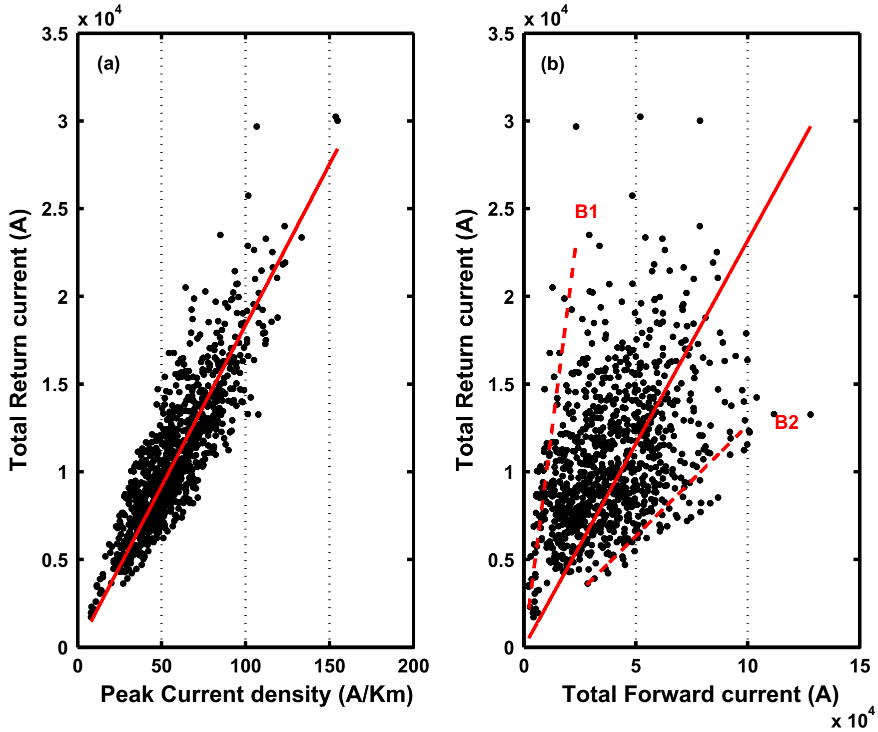

Fig. 7. Scatter plot showing the variation of total return current with (a) peak current intensity and (b) total forward current along with the fitted linear regression line (red solid line) and the boundaries of the scatter (red dashed lines). (For interpretation of the references to colour in this figure legend, the reader is referred to the web version of this article.)

(solid red line) is found to be 0.25. It can be noticed that the variance in the scatter increases with increase in the value of forward current. This indicates the heteroscedastic behaviour of the scatter. Statistical tests of significance used in the linear regression analysis are not valid for such type of data set, as they assume a constant variance in the scatter. Therefore, we have not estimated the significance levels of the fitted line, instead, we have plotted the boundary lines B1 and B2 (red dashed lines). These boundary lines are obtained by fitting linear regression lines through the points of maximum variance on either side of the solid red line. The slopes of lines B1 and B2 are found to be 1 and 0.1 respectively. This indicates that the return current can have values ranging from 0.1 to 1.0 times the forward current. This means that the return current can be equal to forward current or it can be as low as 0.1 times the forward current. The hemispheric asymmetry in the EEJ current is investigated by calculating the forward and return currents in both northern and southern hemispheres separately. In Fig. 6, the area enclosed by the curves C_1DO and C_2DO are considered as the total forward currents in southern and northern hemispheres respectively. Similarly, the area enclosed by the curves $A_1B_1C_1$ and $A_2B_2C_2$ are the total return currents respectively in the southern and northern hemispheres. Both forward (Fig. 8a) and return (Fig. 8b) currents in northern and southern hemispheres show a nearly linear variation, with a slope of 1.0 for forward and 0.95 for return currents. In these scatter plots also one can observe the increase in variance with the increase in current values suggesting heteroscedastic behaviour. Therefore, we have plotted the upper and lower boundaries (red dashed lines) as described in the previous paragraph. The slopes of the upper and lower boundaries for the forward current are found to be 2.3 and 0.67 respectively. This indicates that the forward currents in the northern hemisphere can vary between 0.67 and 2.3 times that in the southern hemisphere. Similarly, for the return currents, the slopes of the boundaries are 2.0 and 0.46. Thus, the values of forward and return currents in the northern hemisphere can be as low as half or as high as double of that in the southern hemisphere, suggesting strong hemispheric asymmetry. These observed hemispheric asymmetries might have seasonal and LT dependence, which will be worth examining. However, due to limited dataset used in the present analysis, it is not possible to study in the present paper and will form the part of the future studies.

3.5. Longitudinal variation

The longitudinal variation of the running average of different EEJ parameters is detailed in this section. Here, the average values of EEJ parameters are computed for a longitudinal window of 30°, stepping forward by 15°, with three-points smoothing. The error bars shown here represent the standard error.

Firstly, we present the longitudinal variation of the average values of the amplitude and the width of EEJ estimated at the ground and is shown in Fig. 9. Earlier studies have

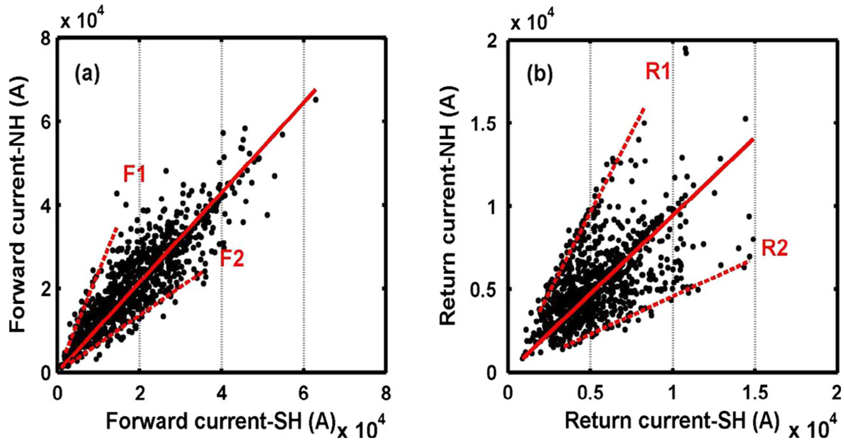

Fig. 8. Scatter plot showing the variation of (a) forward current and (b) return current in the northern hemisphere (NH) and the southern hemisphere (SH) along with the fitted linear regression line (red solid line) and the boundaries of the scatter (red dashed lines). (For interpretation of the references to colour in this figure legend, the reader is referred to the web version of this article.)

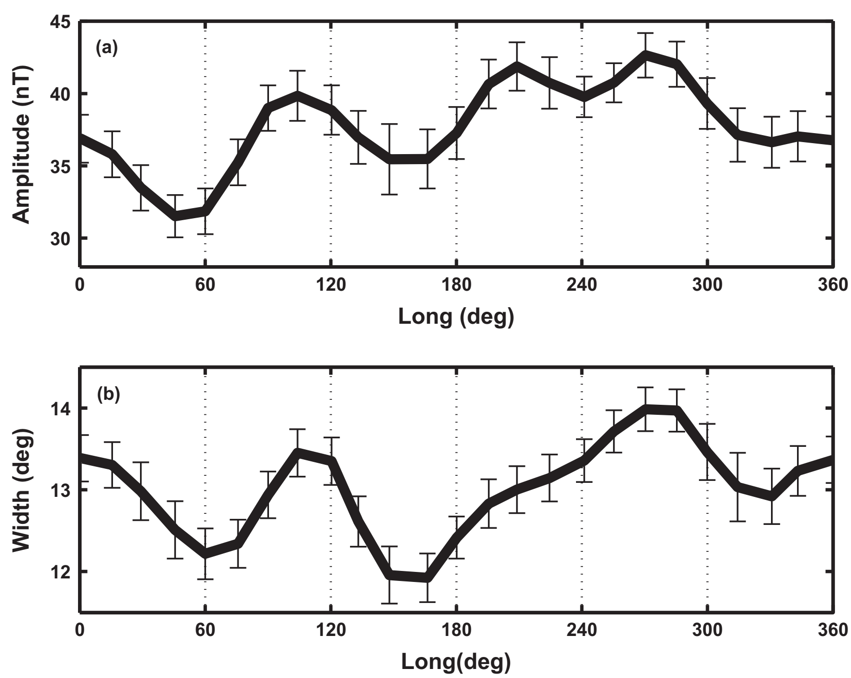

Fig. 9. Longitudinal variation of EEJ (a) strength and (b) width at ground.

shown that EEJ undergoes a strong variability in its amplitude and shows peaks at different longitudes. As indicated by the previous researchers, these peaks in EEJ could be due to the tidal winds in the E-region ionosphere (England et al., 2006; Fang et al., 2009; kil et al., 2011). Various studies have indicated the influence of non-migrating tides on EEJ (Jadhav et al., 2002; Alken and Maus, 2007; Lühr et al., 2008, 2012). Diurnal Eastward wave number 3 (DE-3) non-migrating tides are found to have a major effect on EEJ resulting in a 4-peak structure in the EEJ amplitude during the major part of the year. In the present paper, we found that the EEJ amplitude using Swarm observations also reveal four peak structure (Fig. 9a). The noted peaks at ∼0°, 100°, 200° and 270°E are well in agreement with the earlier observations using Ørsted (Jadhav et al., 2002) and CHAMP (Lühr et al., 2008) and by the climatologically model of EEJ (Alken and Maus, 2007). The width of EEJ (Fig. 9b) estimated at the ground also show similar structure, although peak at 200° is not clear.

Fig. 10 shows the longitudinal variation of the latitudinal extent of forward and return currents of EEJ. The locations of the boundaries of forward current marked as C1 and C2 in the current density profile in Fig. 6 are considered as the latitudinal extent of forward current. The average variations of these boundaries in both northern and southern hemispheres are shown in Fig. 10b and c respectively. Similarly, Fig. 10a and d show the average location of the return current peaks (location of B1 and B2 in Fig. 6) in both the hemispheres. The forward current band is

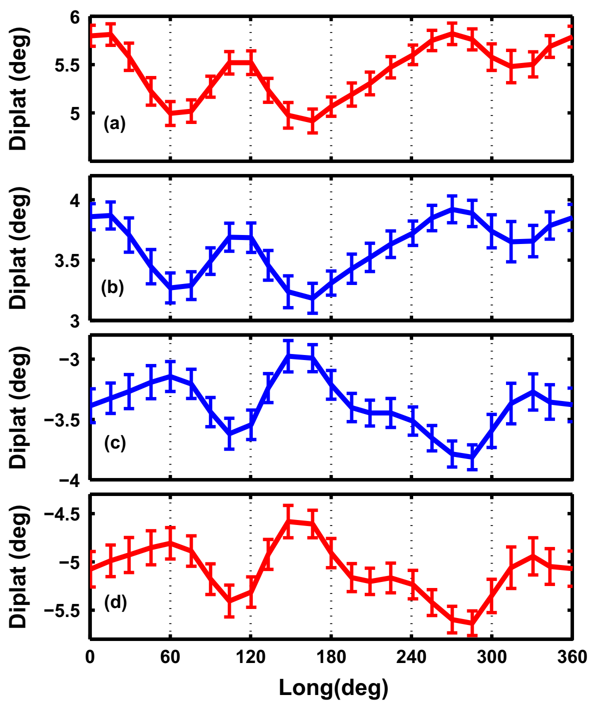

Fig. 10. Longitudinal variation of the locations of the boundary of forward current (b and c) and the locations of the return current peaks (a and d) in both the hemispheres.

observed to have a latitudinal width of ±4° and the return current is found to peak between ±4° to ±6° dip latitudes. These observations are in accordance with Lühr et al. (2004). Fig. 10 shows that the latitudinal extent of the current band (including both forward and return currents) exhibits a longitudinal variation, showing a multi-peak structure. The variations in the southern and northern hemispheres show clear peaks at ~0°, 110° and 270° longitudes. The location of these peaks matches well with the longitudinal variation of EEJ amplitude and width presented above. A small peak at 220° can be seen in the southern hemisphere, which is completely absent in the northern hemisphere. In general, the variations in the northern and the southern hemisphere are found to be consistent with each other.

3.6. Local time variation

Fig. 11 depicts the LT dependence of the mean EEJ amplitude (Fig. 11a) and the mean deviation of EEJ axis from the dip equator (Fig. 11b). Here the hourly mean values are calculated using the observations from satellite passes over all longitudes. Fig. 11a shows a clear local time variation of the EEJ amplitude, peaking near noon. It is observed that EEJ axis slightly shifts away from the dip equator during morning and afternoon hours. The deviation in EEJ axis is found to be anti-correlated with EEJ amplitude, i.e., when EEJ axis is away from the dip, the amplitude of EEJ at the ground is found to be small. This shows the dependence of EEJ amplitude on the location of EEJ axis.

4. F-region currents

In the previous section, we have estimated the westward currents flowing at the off-equatorial location, which can be considered as horizontal return currents of EEJ. It is also possible to have vertical return currents (meridional currents) as suggested by Maeda et al. (1982). Therefore, it is required to examine the vertical extent of the EEJ current system. Since LEO satellites fly in the F-region, it is possible to detect in-situ currents. Using Ampere's Eq. (7), one can estimate the northward (Jx- positive northward), zonal (Jy- positive eastward) and vertical (Jz- positive downward) current densities, as displayed in Eqs. (7a), (7b) and (7c).

$$\nabla X B = \mu_0 J \tag{7}$$

$$J_x = \frac{1}{\mu_0}\left(\frac{\partial B_z}{\partial y} - \frac{\partial B_y}{\partial z}\right) \tag{7a}$$

$$J_y = \frac{1}{\mu_0}\left(\frac{\partial B_x}{\partial z} - \frac{\partial B_z}{\partial x}\right) \tag{7b}$$

$$J_z = \frac{1}{\mu_0}\left(\frac{\partial B_y}{\partial x} - \frac{\partial B_x}{\partial y}\right) \tag{7c}$$

To estimate vertical currents, it is clear from Eq. (7c) that the first term can be computed by using a latitudinal profile during the satellite pass, but to obtain the contribution from the second term it is required to have a pair of satellites separated in longitude with constant height. Swarm, being the three-satellite constellation, can provide this opportunity. We have selected two noon-time passes during 22 April 2014, when Swarm A and Swarm C were simultaneously located at the same height and separated in the longitude by ~1°. The top panel of Fig. 12 shows the average profiles of Bx, By and Bz components observed by Swarm A (red) and Swarm C (blue). Normally, the profiles of Bx and Bz components are smooth, while By profile often contains small scale variations. Similar observation was also noticed by Lühr et al. (2006). Therefore, we have selected the passes which depict most stable By variations. However, we would like to bring to the notice that in general, the By variations during all the passes with LT near noon hours show similar bipolar signature, which is also in accordance with Lühr et al. (2006). Therefore, the results shown in Fig. 12 can be considered as representative of other passes. The estimated Jz current density is depicted in Fig. 12 along with first and second terms of Eq. (7c) (Fig. 12d,e,f).

The estimated vertical current density, Jz (Fig. 12d) shows a maximum positive value at near equator and peak negative values at off-equatorial latitudes. This indicates a downward flowing current near the dip equator at satellite altitude, and the current turns upward at off-equatorial latitudes in the northern and southern hemispheres. These results are similar to those observed by Lühr et al. (2006), who ignored the second term (dBx/dy) and computed only the first term using single satellite CHAMP. Recently, Lühr et al. (2015) used Ampere's ring integral

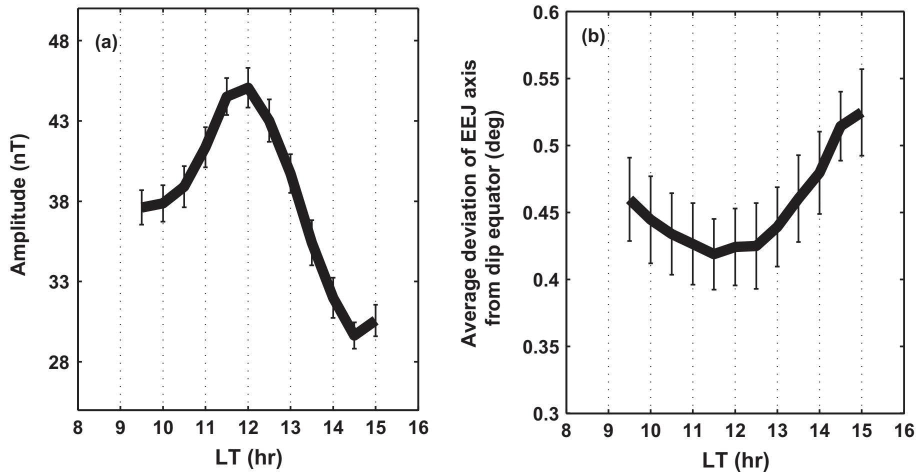

Fig. 11. LT variation of (a) the amplitude of EEJ at the ground and (b) the average deviation of EEJ axis from dip equator.

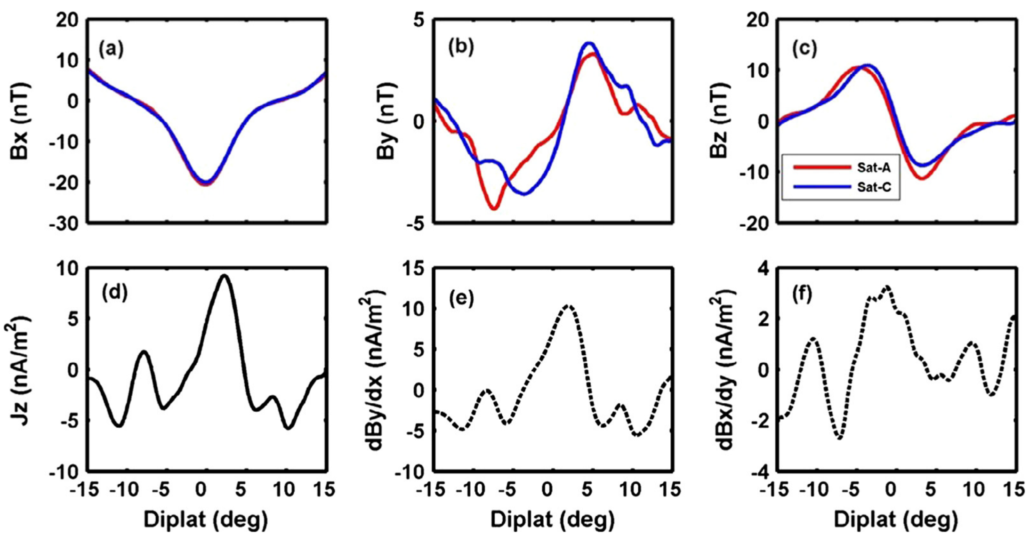

Fig. 12. Vertical currents estimated using Swarm observations. Top Panels show (a) X, (b) Y and (c) Z component of the magnetic field at Swarm A (red solid line) and C (blue solid line) satellites on 22 April 2014. (d) Jz, (e) (dBy/dx) and (f) (dBx/dy) are shown in the bottom panel. (For interpretation of the references to colour in this figure legend, the reader is referred to the web version of this article.)

to estimate the vertical currents, considering the combination of two Swarm satellites and get similar results. According to the meridional current model of EEJ proposed by Maeda et al. (1982), upward currents flowing near dip equator map as downward currents at the off-equatorial latitudes in both the hemispheres. But we are observing opposite directions near noon times, hence the estimated vertical currents might not be related to EEJ current system and can be attributed to meridional currents caused by thermospheric winds flowing in the F-region (Lühr et al., 2006, 2015).

5. Discussion and summary

Magnetic field measurements from LEO satellites form an excellent data base for the study of equatorial electrojet and its global variability. Polar LEO satellites in its transit from pole to pole monitor the EEJ currents flowing at the equatorial latitudes. The magnetic field measurements by these satellites are used to study various parameters of EEJ (Jadhav et al., 2002; Ivers et al., 2003; Lühr et al., 2004, 2008; Alken and Maus, 2007). On a single day, the satellite monitors EEJ flowing over different longitudes around the globe at nearly identical LTs, and hence it is possible to study the longitudinal variability of the current system. To date, different methodologies have been used to derive an understanding of the features of the electrojet currents using various polar LEO satellite missions. Through the present paper, we intent to revisit the problem using an independent dataset from a recent multi-satellite mission Swarm.

In this study, we have fitted an empirical model of electrojet into the Swarm magnetic field observations to obtain the EEJ current parameters, such as peak current density, total forward current, the width of the current system, etc. Unlike the previous studies which fitted empirical model of EEJ assuming symmetry of the EEJ signature in both the hemispheres, present work takes into account the hemispheric asymmetry. Here, we obtain the model parameters separately for both hemispheres. The methodology adopted in finding the current parameters are validated by estimating X variations at Swarm-C using the nearly simultaneous measurements from overhead (longitudinal separation <5°) Swarm-B satellite pass, and comparing with the actual observations from Swarm-C satellite. The current parameters obtained are found to be well correlated with EEJ characteristics such as amplitude and width estimated at the ground. This confirms that current parameters estimated in the present study can be used in investigating EEJ characteristics.

The EEJ have inverted signatures above and below the ionospheric current height. Further, for the first time, we have shown the height dependence of the amplitude and width of EEJ (Fig. 5). It has been demonstrated that with increasing distance from the current layer, the EEJ amplitude decreases and the width increases. The EEJ amplitude at the ground is found to be reduced to ~3/4 of its peak value near current height (~105 km), whereas at satellite altitude (~400 km), the EEJ amplitude is found to be reduced to 1/3 of the peak value. At the same time, the width increases by ~2° at the ground and by ~ 4° at satellites.

The present study also brings out the interesting features of the forward and return currents of EEJ. Return currents estimated are found to be proportional to the peak current density (Fig. 7a), indicating that the current sheet with larger peak current densities has stronger return currents. Return currents also showed a linear variation with forward current, but the scatter is observed to be higher at higher forward current values (Fig. 7b). The forward to return current ratio is found to vary between 0.1 – 1. Also the forward and return currents in the northern hemisphere are found to have values ranging between ~0.5 and 2 times of that in the southern hemisphere suggesting hemispheric asymmetries in the current (Fig. 8). These observed hemispheric asymmetries might have seasonal and LT dependence which can be examined in future studies.

Another important characteristic feature of the EEJ current investigated is its latitudinal extent (Fig. 10). The forward current band is found to have a latitudinal width of ±4° and also shows strong longitudinal variability with four peak structure (Fig. 10b and c). The average locations of the return current peaks vary between ±4° and ±6° dip latitude and are also found to have longitudinal variation similar to forward currents in both the hemispheres (Fig. 10a and d). The width of the current band is observed to peak at ~0°, 100°, 200°, and 280°E longitudes and is consistent with the longitudinal profile of EEJ current amplitudes estimated using previous LEO missions (Jadhav et al., 2002; Alken and Maus, 2007; Lühr et al., 2008).

The longitudinal variations of the amplitude and the width of the EEJ signature also show four peak structures (Fig. 9a and b). The peaks are found to match well with those of the variations of the latitudinal extend of forward and return current. These variations, as pointed out by the previous researchers, are caused by the strong influence of non-migrating DE3 tidal mode on EEJ (Jadhav et al., 2002; Alken and Maus, 2007; Lühr et al., 2012). It has been noticed by several researchers that the tidal modes have strong seasonal dependence. Therefore, it would be more useful to carry out the analysis for different seasons separately. However, with just one and half year data from Swarm satellites there is no good local time coverage for all the seasons and hence, we could not examine this feature.

Although polar LEO satellite cannot witness the day-to-day temporal variation of EEJ, the average variation of electrojet features with LT can be investigated with the considered data set of one and half years during which satellite witnesses all LTs nearly 5 times. The amplitude of EEJ estimated at ground showed a clear LT dependence, with amplitude peaking near noon (Fig. 11a). The average location of EEJ axis is also observed to have LT dependence (Fig. 11b). During noon hours when electrojet strength is observed to be maximum, the axis is found to be located closest to the dip equator, whereas during morning and evening hours EEJ axis deviates from the dip equator. So, it can be inferred that the weak EEJs appear to have axis slightly away from the dip equator. These observations are also in accordance with the previous studies (Fambitakoye and Mayaud, 1976; Jadhav et al., 2002).

The vertical currents estimated using simultaneous observations from Swarm A and Swarm C satellites (Fig. 12) were found to flow downward over the dip equator and upward at off-equatorial latitudes during noon hours. This indicates the existence of meridional currents at satellite altitude, which may be caused by the thermospheric winds flowing in the F-region (Lühr et al., 2006, 2015).

The characteristic features of EEJ parameters discussed in the present paper are broadly in agreement with those obtained from previous LEO missions. With this background, we aim to carry out further detailed investigations of different current systems associated with EEJ (such as three dimensional structure of meridional currents, thick shell of EEJ current system, etc.).

Acknowledgements

Authors are thankful to European Space Agency for making available the vector magnetic field measurements from Swarm satellites. The data sets used are MAGB_LR_1B and MAGC_LR_1B with 1 Hz sampling rate. We whole heartedly thank Prof. R. Rajaram for all the valuable discussions.

References

Alken, P., Maus, S., 2007. Spatio-temporal characterization of the equatorial electrojet from CHAMP, Ørsted, and SAC-C satellite measurements. J. Geophys. Res. 112, A09305. http://dx.doi.org/10.1029/2007JA012524.

Cain, J., Sweeney, R., 1973. The POGO data. J. Atmos. Terr. Phys. 35, 1231–1247. http://dx.doi.org/10.1186/1880-5981-66-4.

Chandra, H., Sinha, H.S.S., Rastogi, R.G., 2000. Equatorial electrojet studies from rocket and ground measurements. Earth Planet Space 52, 111–120.

Chapman, S., 1951. The equatorial electrojet as detected from the abnormal electric current distribution above I-Iuancayo, Peru, and elsewhere. Arch. Meteorol. Geophys. Bioklimatol. A 44, 368–390.

England, S.L., Maus, S., Immel, T.J., Mende, S.N., 2006. Longitu-dinal variation of the E-region electric fields caused by atmospheric tides. Geophys. Res. Lett. 33, L21105. http://dx.doi.org/10.1029/2006GL027465.

McCreadie, H., 2004. Classes of the equatorial electrojet. In: Reigbar, C. et al. (Eds.), Earth Observation with CHAMP Results From Three Years in Orbit. Springer, Berlin, pp. 401–406.

Fambitakoye, O., Mayaud, P.N., 1976. Equatorial electrojet and regular daily variation SR, II, the centre of the equatorial electrojet. J. Atmos. Terr. Phys. 38, 19–26.

Fang, T.-W., Kil, H., Millward, G., Richmond, A.D., Liu, J.Y., Oh, S.-J., 2009. Causal link of the wave-4 structures in plasma density and vertical plasma drift in the low-latitude ionosphere. J. Geophys. Res. 114, A10315. http://dx.doi.org/10.1029/2009JA014460.

Finlay, C.C., Olsen, N., Tøffner-Clausen, L., 2015. DTU candidate field models for IGRF-12 and the CHAOS-5 geomagnetic field model. Earth Planets Space 67 (1), 1.

Forbes, J.M., 1981. The equatorial electrojet. Rev. Geophys. Space Phys. 19 (3), 469–504.

Ivers, D., Stening, R., Turner, J., Winch, D., 2003. Equatorial electrojet from Ørsted scalar magnetic field observations. J. Geophys. Res. 108 (A2), 1061. http://dx.doi.org/10.1029/2002JA009310.

Jadhav, G., Rajaram, M., Rajaram, R., 2002. A detailed study of equatorial electrojet phenomenon using Ørsted satellite observations. J. Geophys. Res. 107 (A8), 1175.

Kil, H., Kwak, Y.-S., Oh, S.-J., Talaat, E.R., Paxton, L.J., Zhang, Y., 2011. The source of the longitudinal asymmetry in the ionospheric tidal structure. J. Geophys. Res. 116, A09328. http://dx.doi.org/10.1029/2011JA016781.

Lühr, H., Kervalishvili, G., Michaelis, I., Rauberg, J., Ritter, P., Park, J., Merayo, J.M.G., Brauer, P., 2015. The interhemispheric and F region dynamo currents revisited with the Swarm constellation. Geophys. Res. Lett. 42, 3069–3075. http://dx.doi.org/10.1002/2015GL063662.

Lühr, H., Rother, M., Häusler, K., Fejer, B., Alken, P., 2012. Direct comparison of nonmigrating tidal signatures in the electrojet, vertical plasma drift and equatorial ionization anomaly. J. Atmos. Solar Terr. Phys. 75, 31–43.

Lühr, H., Rother, M., Hausler, K., Alken, P., Maus, S., 2008. The influence of nonmigrating tides on the longitudinal variation of the equatorial electrojet. J. Geophys. Res. 113, A08313. http://dx.doi.org/10.1029/2008JA013064.

Lühr, H., Maus, S., 2006. Direct observation of the F region dynamo currents and the spatial structure of the EEJ by CHAMP. Geophys. Res. Lett. 33, L24102. http://dx.doi.org/10.1029/2006GL028374.

Lühr, H., Maus, S., Rother, M., 2004. Noon- time equatorial electrojet: its spatial features as determined by the CHAMP satellite. J. Geophys. Res. 109, A01306.

Maeda, H., Iyemori, T., Araki, T., Kamei, T., 1982. New evidence of a meridional current system in the equatorial ionosphere. Geophys. Res. Lett. 9, 337–340.

Onwumechili, C.A., 1992. Study of the return current of the equatorial electrojet. J. Geomagn. Geoelectr. 44, 1–42.

Onwumechili, C.A., 1997. The Equatorial Electrojet. Gordon and Breach, New York.

Onwumechili, C., Agu, C., 1980. General features of the magnetic field of the equatorial electrojet measured by the POGO satellites. Planet. Space Sci. 28, 1125–1130.

Raghavarao, R., Anandarao, B.G., 1987. Equatorial electrojet and the counter electrojet. Ind. J. Rad. Space Phys. 16, 54–75.

Rastogi, R.G., Chandra, H., Chakrabarty, D., Kitamura, K., Yumoto, K., 2007. Day-to-day variability of the equatorial electrojet current in the South American sector. Earth Planets Space 59, 459–461.

Reddy, C.A., Devasia, C.V., 1981. Height and latitude structure of electric fields and currents due to local east-west winds in the equatorial electrojet. J. Geophys. Res. 86, 5751.

Richmond, A.D., 1973. Equatorial electrojet I. Development of a model including winds and instabilities. J. Atmos. Terr. Phys. 35, 1083–1103.

Sampath, S., Sastry, T.S., 1979. Results from in situ measurements of ionospheric currents in the equatorial region I. J. Geomagn. Geoelectr. 31, 373–379.

Sastry, J.S.G., 1970. Diurnal change in the parameters of the equatorial electrojet as observed by rocket-borne magnetometers. In: Donahue, T.M., Smith, P.A., Thomas, L. (Eds.), Space Research X. North-Holland, Amsterdam, pp. 778–785.

Stenning, R.J., 1985. Modeling the electrojet. J. Geophys. Res. 90, 1705–1720.

Stening, R.J., 1995. What drives the equatorial electrojet? J. Atmos Terr. Phys. 57, 1117–1128.

Sugiura, M., Cain, J.C., 1966. A model equatorial electrojet. J. Geophys. Res. 71, 1869–1877.

Sugiura, M., Poros, D.J., 1969. An improved model equatorial electrojet with a meridional current system. J. Geophys. Res. 74, 4025–4034.

Untiedt, J., 1967. A model of the equatorial electrojet involving meridional currents. J. Geophys. Res. 72, 5799–5810.

Vichare, G., Rajaram, R., 2011. Global features of quiet time counter electrojet observed by Ørsted. J. Geophys. Res. 116, A04306. http://dx.doi.org/10.1029/2009JA015244.

Vichare, G., Bhaskar, A., Ramesh, D.S., 2016. Are the equatorial electrojet and the Sq coupled systems? Transfer entropy approach. Adv. Space Res. 57 (9), 1859–1870.